NRC·CNRC

From Discovery
to Innovation...
De la découverte
à l'innovation...

La Science à l'œuvre pour le
at work for Canada

NRC Publications Archive
Archives des publications du CNRC

Preform Shape and Operating Condition Optimization for the Stretch Blow Molding Process

Thibault, Francis; Malo, Alain; Lanctot, Benoit; Diraddo, Robert

This publication could be one of several versions: author's original, accepted manuscript or the publisher's version. /
La version de cette publication peut être l'une des suivantes : la version prépublication de l'auteur, la version
acceptée du manuscrit ou la version de l'éditeur.
For the publisher's version, please access the DOI link below./ Pour consulter la version de l'éditeur, utilisez le lien
DOI ci-dessous.

NRC Publications Record / Notice d'Archives des publications de CNRC:
http://nparc.cisti-icist.nrc-cnrc.gc.ca/npsi/ctrl?action=rtdoc&an=11343961&lang=en
http://nparc.cisti-icist.nrc-cnrc.gc.ca/npsi/ctrl?action=rtdoc&an=11343961&lang=fr

Contact us / Contactez nous: nparc.cisti@nrc-cnrc.gc.ca.

National Research
Council Canada
Conseil national
de recherches Canada

Canada

Preform Shape and Operating Condition Optimization for the Stretch Blow Molding Process

F. Thibault, A. Malo, B. Lanctot, R. Diraddo

Industrial Materials Institute, National Research Council of Canada, Boucherville, Québec J4B 6Y4, Canada

In this work, a new design approach was developed to automatically and consecutively predict optimal preform geometry and optimal operating conditions for the stretch blow molding process. The numerical approach combines a constrained gradient-based optimization algorithm that iterates automatically over predictive finite element software. The strategy allows for targeting a specified container thickness distribution by manipulating consecutively the preform geometry (thickness and shape) and the operating parameters subject to process and design constraints. For the preform shape optimization, the preform geometry is mathematically parameterized for simplified treatment and the corresponding sensitivities are evaluated using a finite difference technique. A finite difference technique is also employed for the operating condition optimization. The constrained optimization algorithms are solved via the use of the sequential quadratic programming method that updates the design variables accordingly. Predicted optimization results obtained on an industrial case are presented and discussed to assess the validity when compared to experimental results and the robustness of the proposed approach. POLYM. ENG. SCI., 47:289–301, 2007. © 2007 Society of Plastics Engineers

INTRODUCTION

Stretch blow molding (SBM) is the process of choice for the production of PET containers, in particular for the food and beverage industry as well as the pharmaceutical sector. The SBM process is a high volume process with costly tooling for both the preform and the container. For example, an injection-molding machine can have a 144-cavity preform configuration and a stretch blow-molding machine can have a 16-cavity blow molds. Therefore, it is critical in the design phase to minimize tooling modifications, which can be quite costly.

The design of the tooling in polymer processing via the use of modeling technologies has increased significantly in industry over the last 10 years. The drivers for their use are reduced part development time, improved part quality, and minimized tooling modifications. Recently, for injection molding, FEM simulation tools have been integrated into automatic optimization algorithms [1] in an effort to mimic a design engineer's ideal use of the software. For SBM, simulation tools have recently begun to penetrate into the culture of the industrial design process. The subsequent integration of these simulation tools into numerical optimization algorithms for automatically predicting preform shape geometries and operating conditions would significantly assist in the development cycle.

The SBM process involves three stages, the reheat stage where previously injection-molded preforms are heated to the desired forming temperature distribution, followed by blowing and the solidification stages. During the blowing stage, the preform is stretched with a cylindrical rod. For the duration of stretching, a pre-blow is applied to prevent the stretching rod from contacting the inside preform wall, which can lead to container defects. When the rod reaches the bottom wall of the container, a high blow pressure is applied inside the preform to reach the final container shape and maximize cooling efficiency. The high pressure is held for ~1 or 2 s to cool the container down and an exhaust is finally performed to get the final product.

The design space for numerical optimization is highly complex. The process sequence is complex and highly coupled, resulting in major challenges regard to prediction and subsequent optimization. The material rheological behavior during the stretching and inflation steps is highly nonlinear and thermally dependent, resulting in further challenges with regard to prediction and subsequent optimization. Furthermore, the optimization strategy needs to consider process and design constraints, which further complicate the calculation.

From a numerical optimization point of view, only the work of Lee and Soh [2] has been reported in the literature for SBM. They developed a finite element optimization method to determine the optimal thickness profile of a preform for a blow-molded part, given the required wall thickness distribution. In their approach, the preform was not axially stretched during the forming stage and only one manufacturing constraint is applied, that being the ejection of the preform from the mold. As there was no axial preform stretching and no constraint about the core-rod ejection during the injection molding process, the model, although a
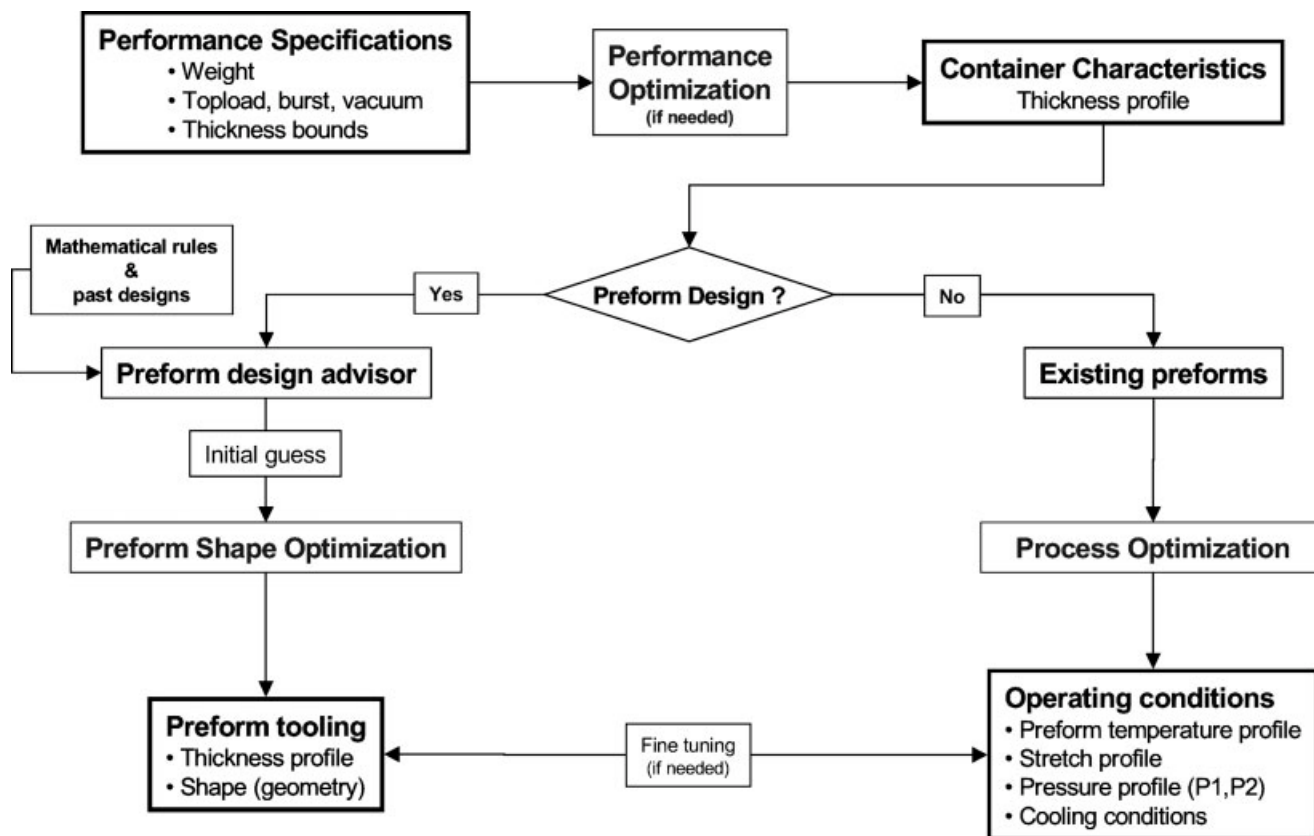
FIG. 1.   Schematic overview of preform design strategies.

good first step, did not include important steps in the process sequence.

Other related optimization works have been published in extrusion blow molding. Laroche et al. [3] proposed a closed-loop optimization approach analogous to classical process control system to manipulate the process parameters such as the die programming profile to obtain desired target values of inflated part thickness. Gauvin et al. [4] revisited the previous work by employing a gradient-based approach to minimize the design objective function by manipulating the processing parameters.

In polymer injection molding, Smith et al. [5] and Kabanemi et al. [6] used a design sensitivity analysis coupled with a gradient-based approach to optimize the gate location in order to minimize filling time. Several papers in metal forming [7–12] have proposed different shape optimization algorithms to optimize the preform die shape to get final part with a pre-specified geometry. The shape optimization integrating the finite element analysis tools is an emerging field with a strong potential and will be addressed in this work.

Optimization Design Environment

The goal of this work was to develop a design optimization environment for the design of preforms and container moulds. Throughout the optimization, the strategy considers the coupled effects of the different steps in the blowing sequence as well as highly nonlinear and thermally dependent material behavior.

Two complementary optimization algorithms are proposed in this work:

- Preform shape optimization that manipulates the preform geometry (shape and thickness) for a given set of processing conditions to target the desired container thickness distribution.
- Operating condition optimization that manipulates the operating parameters for a given preform geometry to target the required container thickness distribution.

The optimization strategies are integrated into a design environment as illustrated in Fig. 1. A performance optimization is performed to predict the container thickness distribution that minimizes the preform weight and satisfies performance specifications such as top load, pressurization, and vacuum loads.

The next step involves making a decision as to whether or not a new preform has to be designed to satisfy the predicted container thickness distribution. To minimize the cost associated with the design of a new preform, designers prefer to use existing preforms and adjust or optimize the operating conditions to satisfy the container performance. In this scenario, an operating condition optimization is triggered.
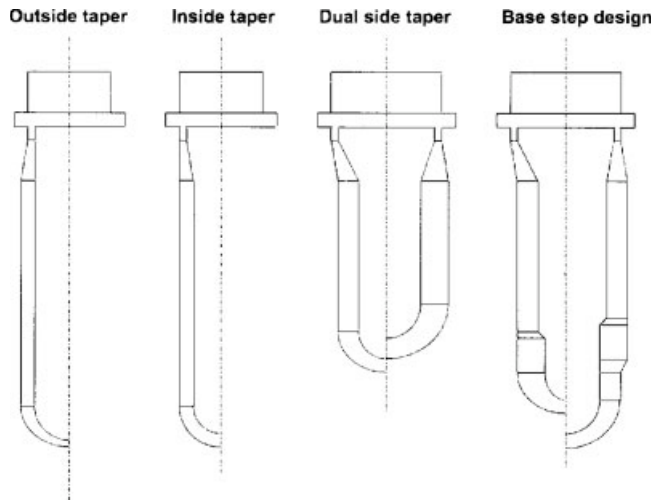
FIG. 2. Different types of preform geometry used in the industry (Courtesy of CRC Press).

If the container thickness targets cannot adequately be reached, a new preform must be designed using the preform shape optimization, which would precede the cutting of a new preform mould. Finally, once the preform shape optimization is complete, a final operating condition optimization is performed in order to fine-tune the operating conditions further. As preforms are injection molded, their design geometry must take into account constraints such as core rod demouldability from the inside preform and preform demouldability from its cavity. Different types of preform
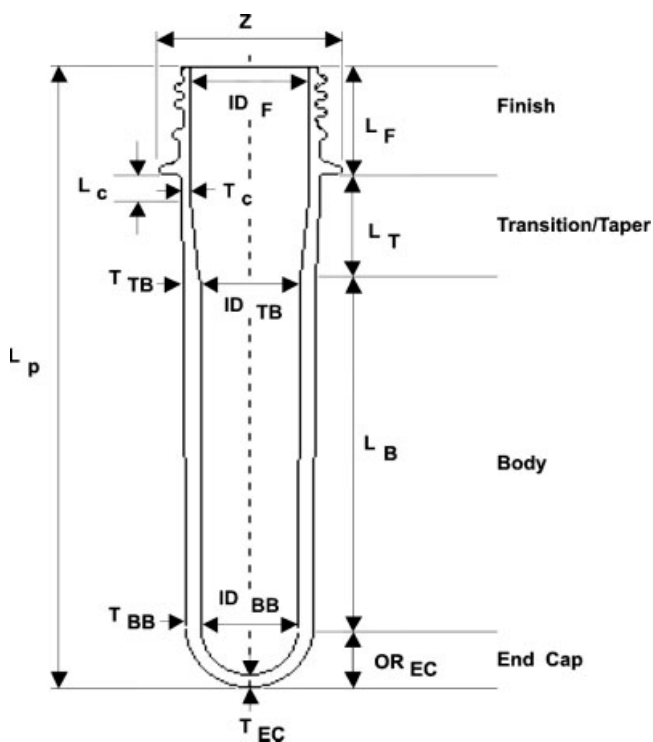

FIG. 3. Parameterization of preform into four sections: finish, taper, body, and end-cap.

are used in the industry to satisfy these constraints (Fig. 2). In this work, we focus on the first three preform types (outside, inside, and dual side taper preforms) that represent around 85% of all the preforms designed in industry.

The preform is divided into four sections: finish, taper, body, and end-cap sections. These sections have been parameterized to efficiently allow for reconstruction of the entire preform geometry after every optimization iteration, by modifying one or more of these parameters (Fig. 3). The variables l, ID, Z, T, and OR represent the length, the inside diameter, the finish outside support ledge, the thickness, and the outside radius of the preform, respectively. The indices f, tp, c, TB, BB, and EC represent the finish, the total preform, the conveying zone, the top body, the bottom body, and the end-cap, respectively.

The geometric relationship between container and preform is illustrated in Fig. 4. From a design point of view, three different types of stretch ratios are usually considered in the preform design [13]: axial stretch ratio (λ_{ax}), hoop stretch ratio (λ_h), and end-cap thickness ratio (δ). The axial stretch ratio is the ratio of the bottle length (L_b) to the preform length (l_p), without taking into account the finish length that is not generally considered to be an active stretched region. The hoop ratio is defined as the ratio of the outside diameter of the container (D_b) to the outside diameter of the preform (d_b). The end-cap thickness ratio represents the ratio of the bottom body thickness to the end-cap thickness. For example, for a typical 2 L carbonated soft drink (CSD) bottle, these stretch ratios range in the next preform design window [13]:

$$2.2 < \lambda_{ax} < 2.8,$$
$$4.4 < \lambda_h < 5.4,$$
$$0.7 < \delta < 0.8. \qquad (1)$$

The product of axial and hoop ratios gives the total blow up ratio (BUR), which is an indication of the total stretched ratio undergone by the PET material during the forming pro-
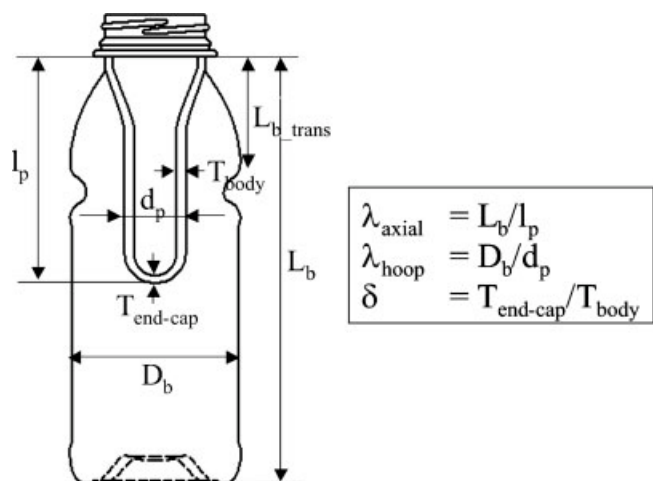

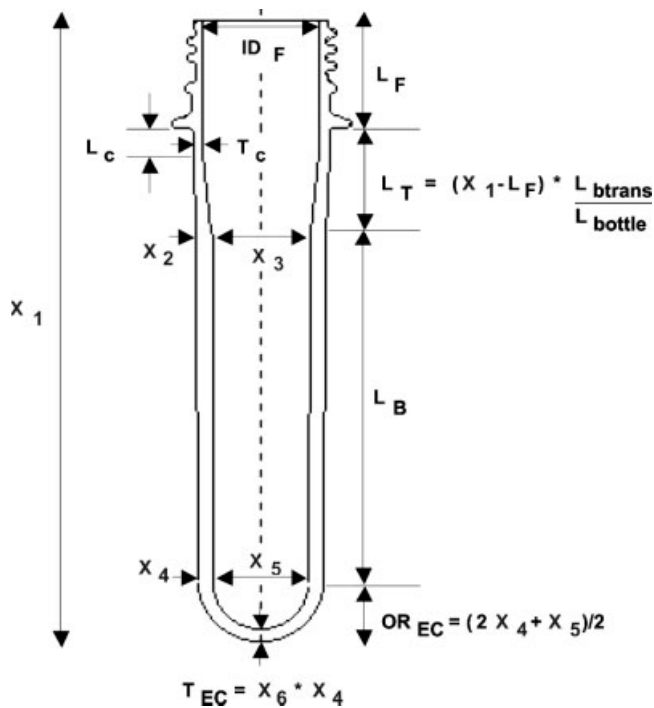FIG. 4. Relationship between container and preform in term of stretch ratios.

FIG. 5. Preform shape optimization design variables (X_1 to X_6).

cess. The BUR could vary significantly depending on the bottle types manufactured (hot fill, CSD, or water). The industry is constantly aiming for higher BUR value in order to improve PET bottle mechanical and barrier properties that strongly influence by an increase of material molecular orientation. However, care has to be taken to avoid polymer overstretching or polymer delaminating during the forming process.

NUMERICAL FORMULATION

The first step in numerical design stage is the mathematical formulation of the objective function. The purpose of the objective function is to numerically describe in one expression, the part specifications, the design variables, and the costs associated with processing and part quality. It consists of the minimization of a cost function, subject to a series of inequality, equality, and bound constraints that limit the design space by automatic manipulation of a series of design variables (**X**). The problem definition can be expressed as the following:

Minimize the objective function

$$F(\mathbf{X}) \qquad (2)$$

subject to
- Inequality constraints or specifications

$$g_j(\mathbf{X}) \leq 0, \quad j = 1, m. \qquad (3)$$

- Equality constraints or specifications

$$h_k(\mathbf{X}) = 0, \quad k = 1, n. \qquad (4)$$

- Side constraints or design variable limits

$$\mathrm{X}_{i,\min} < \mathrm{X}_i < \mathrm{X}_{i,\max}, \quad i = 1, p \qquad (5)$$

by manipulating the design variables $X = \{X_1, X_2, \ldots, X_p\}$.

Once the objective function is defined, a numerical optimization can be performed using a variety of available techniques such as traditional gradient techniques of zero, first, and second order or soft computing methods [14]. In this work, a second order method (sequential quadratic programming (SQP)) of the design optimization tools (DOT) has been used due to its strong track record [14]. The numerical optimization iterates over a simulation tool as it moves towards the optimal condition.

The optimization algorithms developed in this work integrate finite element SBM simulations that model the preform material deformation during the consecutive process stages. The Blow-View software technology from National Research Council of Canada has been used to model the SBM process [15, 16, 17].

The simulation phases include reheat, conditioning, stretching, and inflation preform deformation and cooling. The process modeling is based on a large displacement nonlinear finite element formulation [18]. The finite element mesh of the initial preform is created based on the preform parameterization information. The preform deformation is modeled using a multilayer membrane element type and a nonisothermal hyper-viscoelastic material model. The hyper-viscoelastic deformations are modeled using a modified Christensen–Yang-like model proposed by Pham et al. [15] that gives the true stress σ of the PET material as a function of the strain history according to
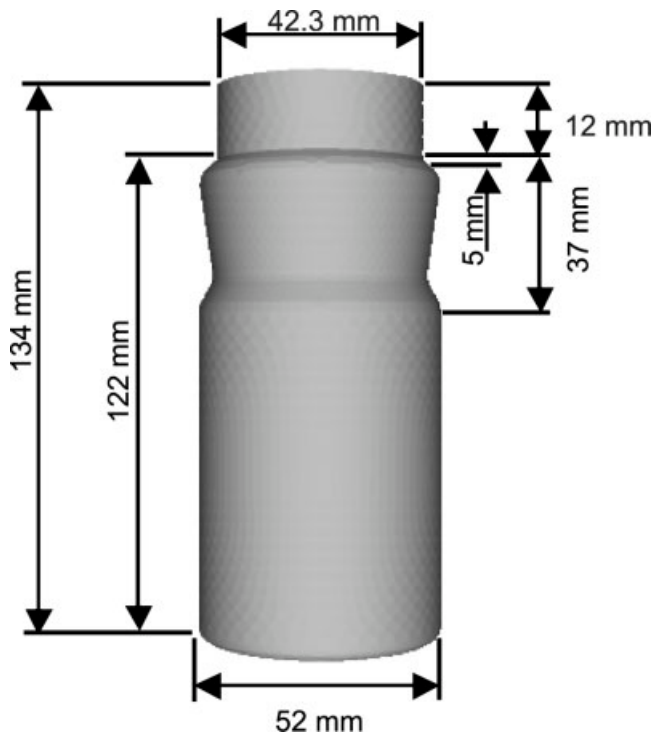

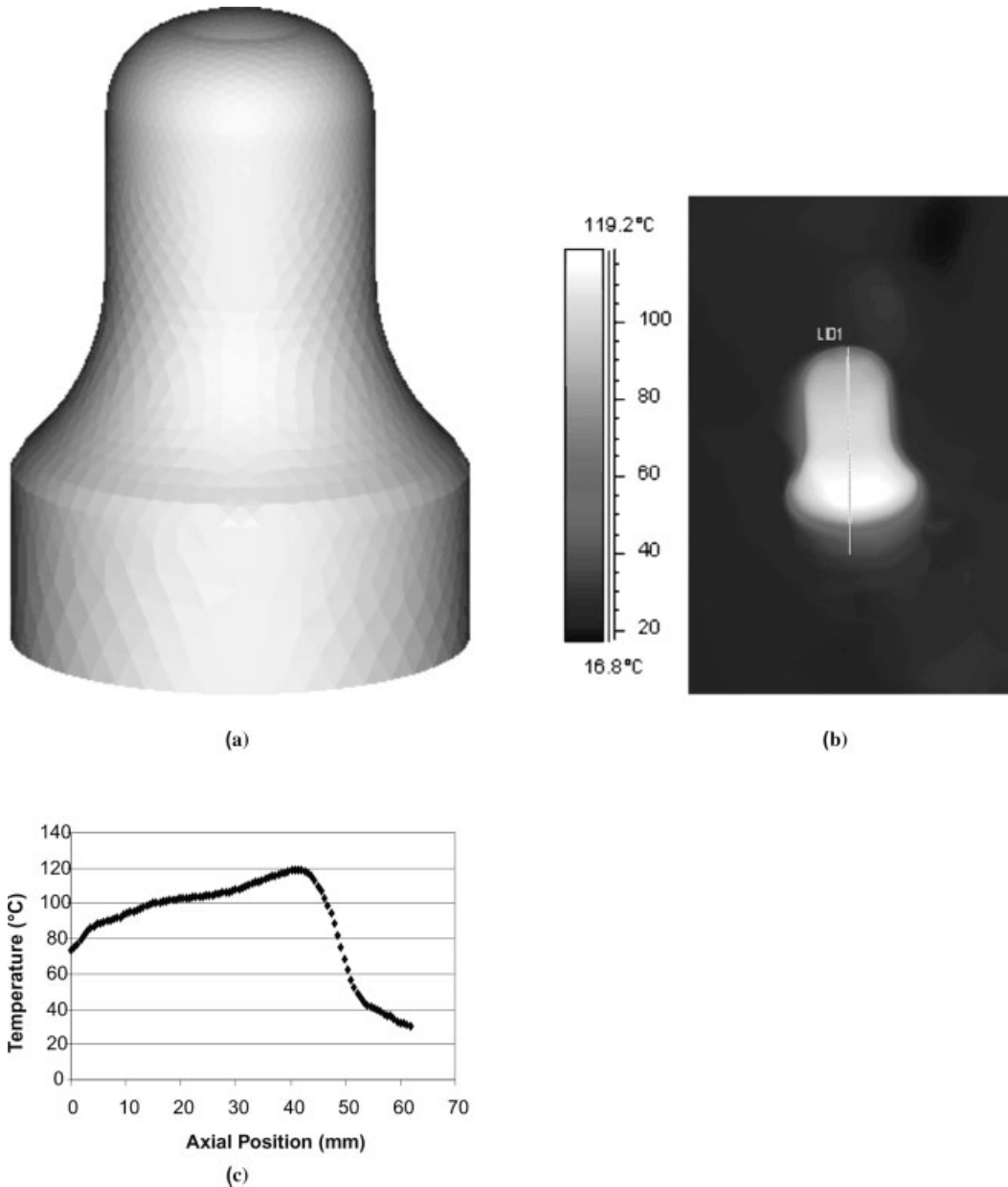FIG. 6. Dimensions of spice jar container of Husky company.

FIG. 7.   Initial preform temperature profile measured from infrared camera before entering the blow station.

$$\boldsymbol{\sigma} = -p\boldsymbol{\delta} + 2\{M_1 + M_3(I_2 - 3)\}\mathbf{c}^{-1} - 2\{M_2 + M_3(I_1 - 3)\}\mathbf{c}$$
$$+ \mathbf{F}(t)\left\{\int_0^t \{M_4 + M_5 I_2\} \exp\left(-\frac{t-\tau}{M_6}\right)\dot{\mathbf{E}}d\tau\right\}(^T\mathbf{F}(t)) \quad (6)$$

where $\mathbf{c}^{-1}$, $\mathbf{c}$, p, $\dot{\boldsymbol{E}}$, $\boldsymbol{F}(t)$, and M_i are the Finger, left Cauchy–Green deformation tensors, the arbitrary hydrostatic pressure, the gradient tensor, the strain rate tensor, and the model parameters, respectively.

Preform Shape Optimization

Each objective function evaluation requires the automatic creation of a finite element mesh of the preform and a subsequent performing of a nonlinear finite element analysis of the SBM process.

The following objective function is evaluated at the end of the forming stage

$$\sigma(X)^2 = \sum_{i=1}^{N_e}(T_i - T_t(y))\frac{\Omega_i}{\Omega} \quad (7)$$

which represents the container thickness variance around thickness targets (T_t) defined by the designer along the container in y direction. N_e and T_i correspond, respectively, to the number of finite elements in the preform mesh and the nodal finite element thickness. The variance is weighted by the ratio of the local element surface (Ω_i) to the total container surface (Ω), which will not be affected by the mesh topology.

The process constraints can be expressed as the following:

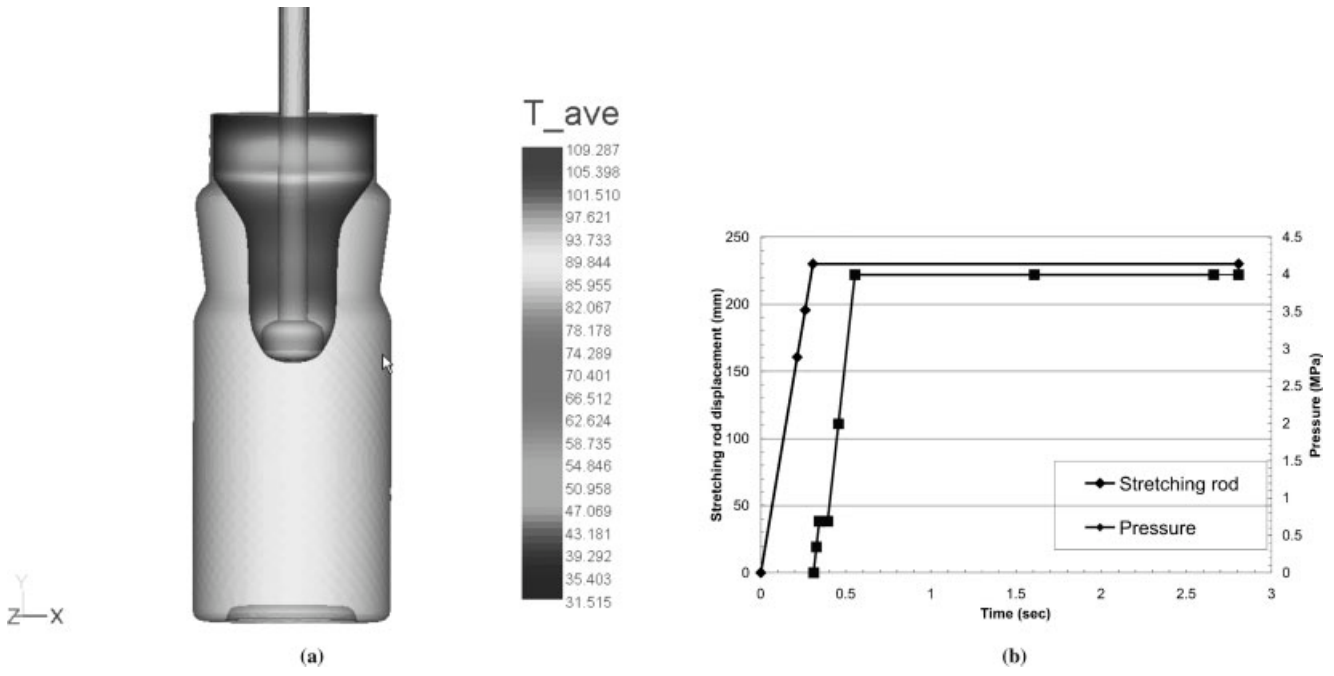• Injection molding demouldability constraints:

FIG. 8. Temperature profile along the preform and processing conditions at the blowing station.

○ core-rod demouldability

$$ID_{BB} < ID_{TB} \qquad (8)$$

$$ID_{BB} < ID_F \qquad (9)$$

$$ID_{TB} < ID_F \qquad (10)$$

○ preform demouldability

$$OD_{BB} < OD_{TB} \qquad (11)$$

$$OD_{TB} < Z \qquad (12)$$

○ nesting (not always required - optional)

$$ID_{TB} < OD_{BB}. \qquad (13)$$

• SBM constraints:
  ○ stretching rod clearance

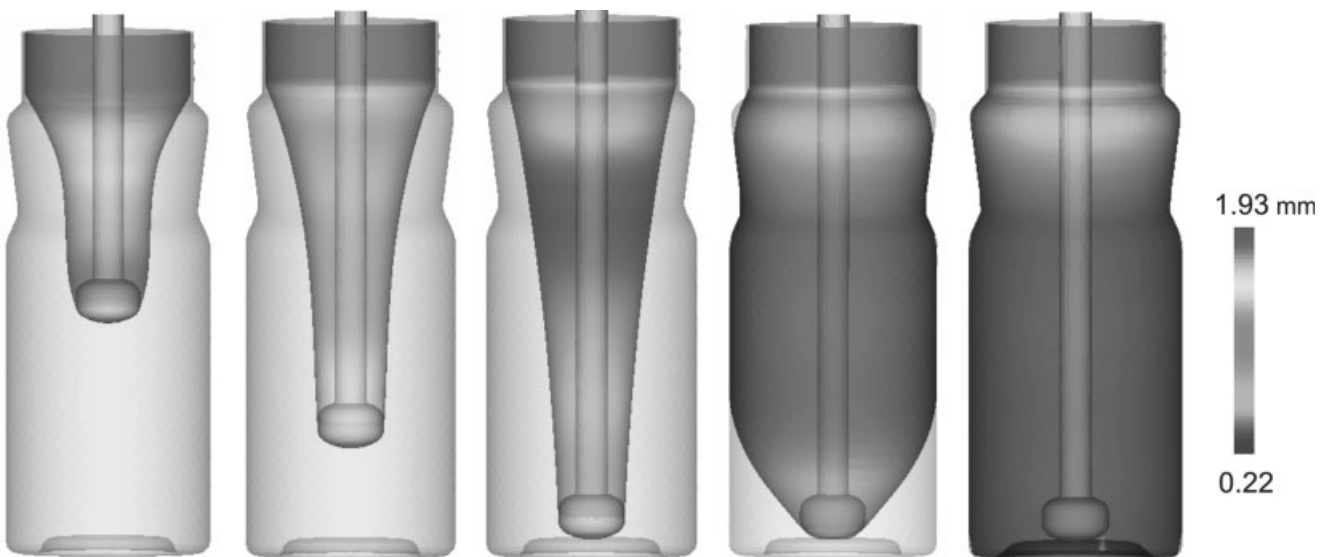$$D_{rod} + R_{Cl} < ID_{BB} \qquad (14)$$

FIG. 9. Typical preform thickness evolution during stretching and blowing into the mould.
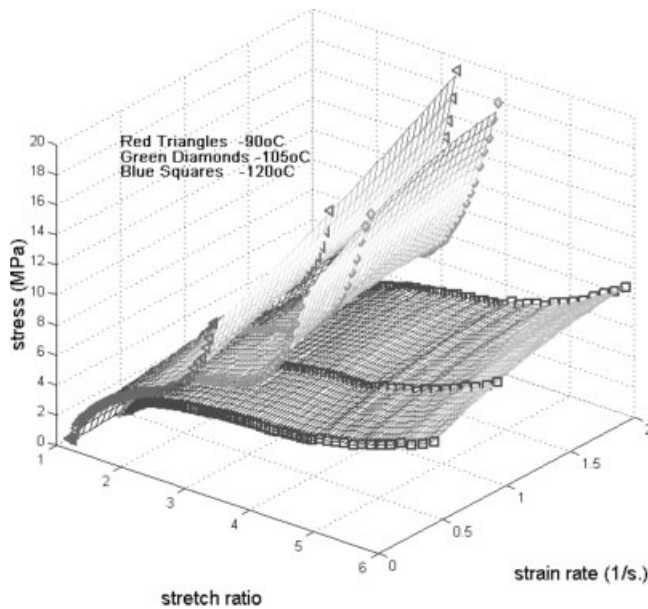
FIG. 10. Experimental material behavior of PET CB12.

$$D_{\text{rod}} + R_{\text{Cl}} < \text{ID}_{\text{TB}} \qquad (15)$$

where R_{Cl} represents the rod clearance ($\sim$1–2 mm). Since constraints 9 and 15 are redundant, they will not be taken into account.

To maintain a balance of efficiency of calculation versus validation of results, only six (Eq. 6) preform design variables will be manipulated to define the preform geometry as shown on Fig. 5. In an ideal case scenario, all radii in the preform taper sections can be added into the list of design variables.

From established design rules, the ratio of the preform transition length (l_{T}) to the active preform length ($l_{\text{p}} = l_{\text{tp}} - l_{\text{f}}$) is proportional to the ratio of the bottle transition length ($L_{\text{b\_trans}}$) to the bottle length (L_{b}). Based on the definition of these preform design variables, the constrained optimization problem can be reformulated as

TABLE 1. Definition of initial preform design variables and design variable limits (lower and upper bounds) for the preform shape optimization.

Design variable name	Lower bound	Initial value	Upper bound
Axial stretch ratio, X'_1	2.5	2.6	2.7
Top body thickness, X_2 (mm)	1.0	2.0	5.0
Inside top body diameter, X_3 (mm)	16.0	22.0	25.0
Bottom body thickness, X_4 (mm)	1.0	2.0	5.0
Inside bottom body diameter, X_5 (mm)	16.0	21.9	25.0
End-cap thickness ratio, X_6	0.667	0.667	0.85

TABLE 2. Comparison between initial and optimal preform geometries.

Design variable name	Initial design	Optimal design
Axial stretch ratio, X'_1	2.6	2.50
Top body thickness, X_2 (mm)	2.0	2.48
Inside top body diameter, X_3 (mm)	22.0	25.0
Bottom body thickness, X_4 (mm)	2.0	2.48
Inside bottom body diameter, X_5 (mm)	21.9	25.0
End-cap thickness ratio, X_6	0.667	0.667
Square root of objective function, σ (mm)	0.159	0.034

Minimize the design objective function

$$\sigma(X)^2 = \sum_{i=1}^{N_e} (T_i - T_t(y)) \frac{\Omega_i}{\Omega} \qquad (16)$$

by manipulating the preform design variables

$$
\begin{aligned}
X'_{1,\text{min}} &< X'_1 < X'_{1,\text{max}} \\
X_{2,\text{min}} &< X_2 < X_{2,\text{max}} \\
D_{\text{rod}} + R_{\text{Cl}} &< X_3 < \text{ID}_{\text{F}} \\
X_{4,\text{min}} &< X_4 < X_{4,\text{max}} \\
D_{\text{rod}} + R_{\text{Cl}} &< X_5 < \text{ID}_{\text{F}} \\
X_{6,\text{min}} &< X_6 < X_{6,\text{max}}
\end{aligned} \qquad (17)
$$

subject to process constraints

$$
\begin{aligned}
X_5 &< X_3 \\
(2X_4 + X_5) &< (2X_2 + X_3) \\
(2X_2 + X_3) &< Z \\
X_3 &< (2X_4 + X_5) \ \text{(optional)}. \quad (18)
\end{aligned}
$$

Instead of manipulating the total preform length (X_1), it is more convenient to manipulate the axial stretch ratio (X'_1
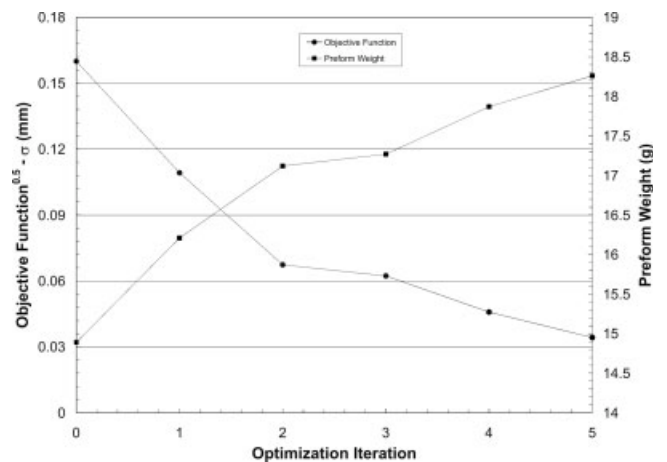

FIG. 11. Objective function and preform weight evolution in function of optimization iterations for the preform shape optimization.
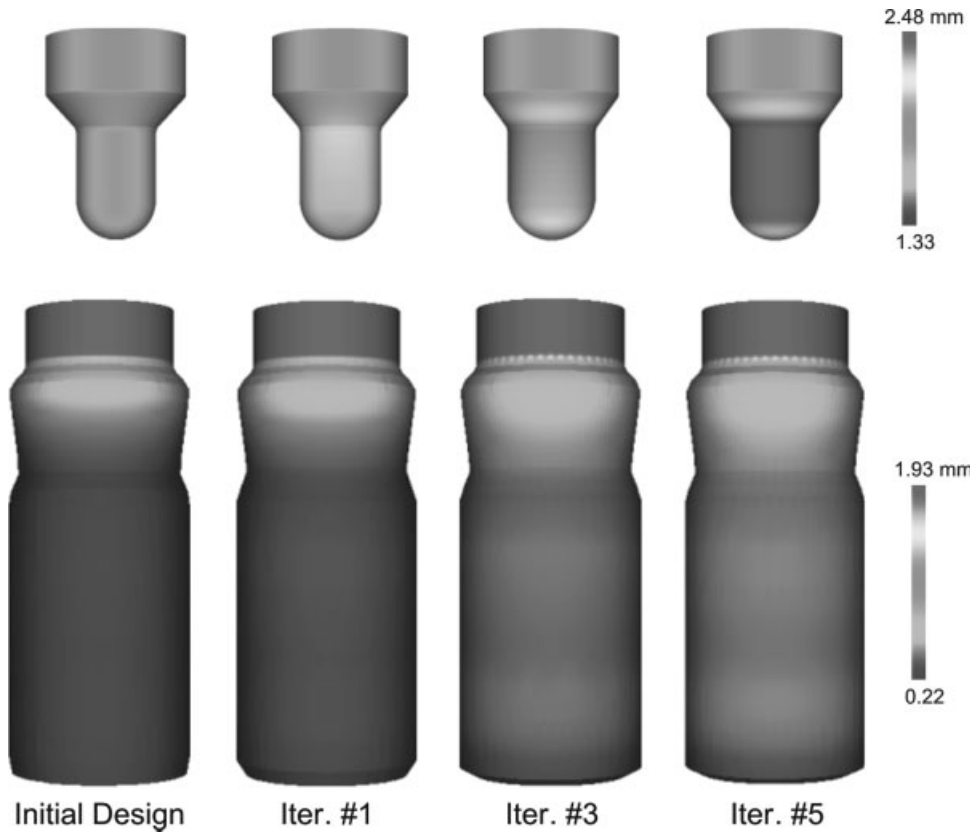
FIG. 12.   Preform-container thickness profiles evolution during the preform shape optimization.

$= \lambda_{ax}$) that is related to the total preform length using the following relationship

$$X_1 = l_p + l_f = L_b/\lambda_{ax} + l_f = L_b/X_1' + l_f. \quad (19)$$

The choice of proper design variable limits allows for satisfying of some of the process constraints (*Eqs. 8, 9, 13, 14*).

Operating Condition Optimization

For the operating condition optimization, the preform geometry is held constant and the selected strategy is to manipulate the processing parameters to target a required container thickness profile. In this work, the following operating parameters are simultaneously manipulated:

- Pre-blow pressure (P_1)
- Blow pressure (P_2)
- Stretching rod speed (V_R)
- Temperature profile along the preform ($T_{P,i}$).

As there are many different types of reheat stations and configurations in the industry, all with varying efficiency levels, it was preferred to manipulate the preform temperature profile before entering the blow station instead of manipulating reheat-processing conditions. In this context, the designer would have to include heuristic know-how on tuning specific ovens to obtain the predicted preform temperature distribution.

For this specific optimization problem, the only constraints are side constraints for each of the design variables. The constrained optimization problem can therefore be reformulated as

Minimize the design objective function

$$\sigma(X)^2 = \sum_{i=1}^{N_e} (T_i - T_t(y)) \frac{\Omega_i}{\Omega} \quad (20)$$
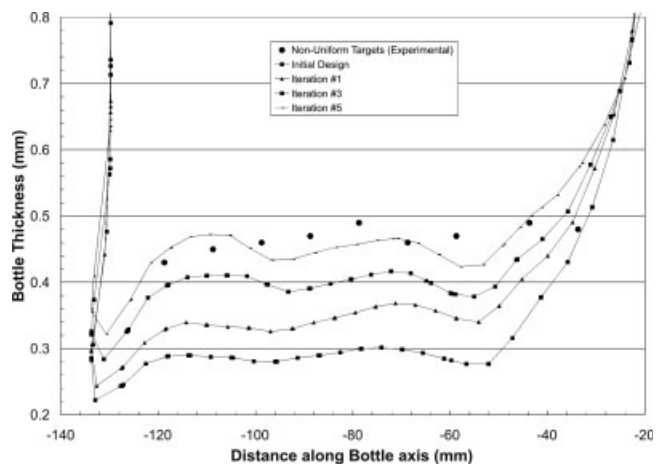

FIG. 13.   Evolution of container thickness distribution in function of optimization iteration for the preform shape optimization.
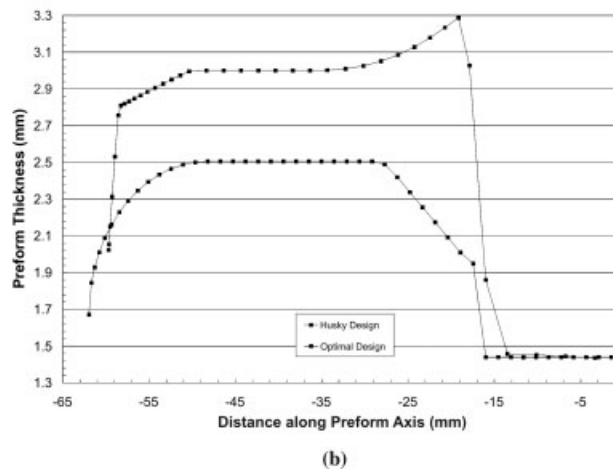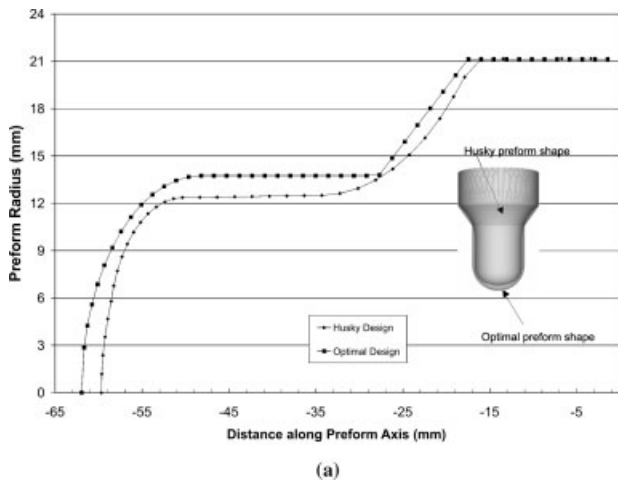
FIG. 14. Preform shape and thickness comparison for optimal and Husky designs.

by manipulating the processing design variables

$$P_{1,\min} < P_1 < P_{1,\max}$$
$$P_{2,\min} < P_2 < P_{2,\max}$$
$$V_{R,\min} < V_R < V_{R,\max}$$
$$T_{p,i,\min} < T_{p,i} < T_{p,i,\max}. \qquad (21)$$

MATERIALS AND EXPERIMENTAL

Experimental validation data for the optimization of a PET preform is obtained through the production of a spice jar container manufactured by Husky Injection Molding Systems (Fig. 6). The initial geometries are also supplied by Husky Injection Molding Systems (HIMS).

The 22 g wide-mouth spice jar was manufactured on a single-stage process using Husky IndexSB stretch blow

FIG. 15. Preform temperature design variables along the Husky preform geometry.

molding machine. The preform temperature profile was measured with an infrared camera just prior to entering the blowing station (Fig. 7). The operating conditions for the blowing stage are illustrated in Fig. 8. The container is a wide-mouth type and the stretching rod is a 16 mm diameter mushroom type. Therefore the preblow pressure is applied shortly after the end of preform stretching quickly followed by the final blow pressure, since there is no risk for the rod to contact the preform wall in that situation. The high pressure is maintained for ~2 s while cooling the container down. Figure 9 shows a typical preform thickness evolution during stretching and blowing into the mould.

The PET material used was Voridian CB12. The grade has been characterized on a biaxial stretcher (Bruckner) using equi-biaxial stretching experiments [15]. Samples of dimensions of $85 \times 85 \times 1.5$ mm^3 were heated up to the desired characterization temperature and simultaneously stretched in both directions (MD and TD). The corresponding results at different temperatures, including strain hardening in the stress–strain curve, are shown in Fig. 10.
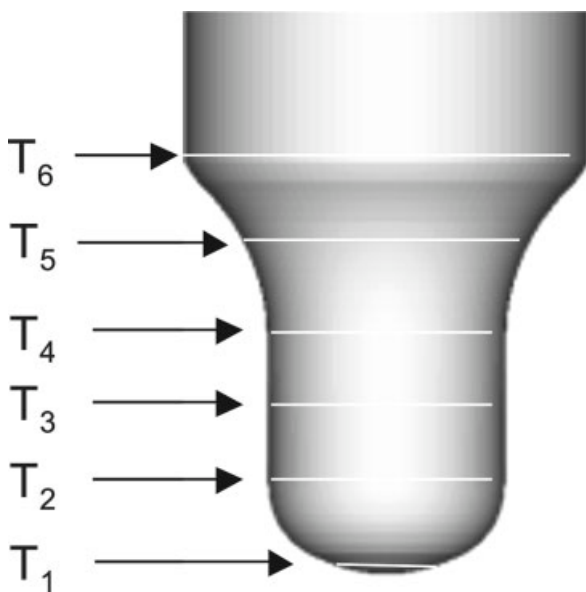
CASE STUDIES

Preform Shape Optimization

The first optimization involves manipulation of the preform geometry to target a nonuniform container thickness

TABLE 3. Definition of initial temperature design variables and design variable limits (lower and upper bounds) for the process optimization.

Design variable name	Lower bound	Initial value	Upper bound
Preform temperature at position 1, X_1 (°C)	40.0	65.0	120.0
Preform temperature at position 2, X_2 (°C)	70.0	95.0	120.0
Preform temperature at position 3, X_3 (°C)	80.0	95.0	120.0
Preform temperature at position 4, X_4 (°C)	80.0	105.0	120.0
Preform temperature at position 5, X_5 (°C)	80.0	105.0	120.0
Preform temperature at position 6, X_6 (°C)	60.0	75.0	120.0

TABLE 4. Comparison between initial and optimal preform temperature profiles.

Design variable name	Initial design	Optimal design
Preform temperature at position 1, X_1 (°C)	65.0	64.0
Preform temperature at position 2, X_2 (°C)	95.0	94.2
Preform temperature at position 3, X_3 (°C)	95.0	102.0
Preform temperature at position 4, X_4 (°C)	105.0	100.0
Preform temperature at position 5, X_5 (°C)	105.0	120.0
Preform temperature at position 6, X_6 (°C)	75.0	72.6
Square root of objective function, σ (mm)	0.110	0.032

FIG. 17. Evolution of container thickness distribution in function of optimization iteration for the first process optimization.

distribution. The container thickness profile targeted is the experimental thickness distribution obtained by HIMS. This will allow for subsequent comparison of the optimal preform geometry obtained in this work to the Husky preform design. Table 1 lists the initial preform design variables and the preform design variable limits (lower bounds and upper bounds) for the case studied. The initial preform body thickness (X_2) has been decreased significantly in an effort to test the optimization algorithm.

The results are shown in Table 2 and Figs. 11–13. The proposed optimization algorithm is able to decrease rapidly the objective function (Fig. 11) from $\sigma^2 = 0.026$ mm^2 ($\sigma = 0.159$ mm) down to $\sigma^2 = 0.00117$ mm^2 ($\sigma = 0.034$ mm) after 5 optimization iterations. No significant improvement is evident after the fifth iteration. At the same time, the preform weight increases from 14.8 to 18.3 g since the preform body thickness has to be increased to properly satisfy the required nonuniform container thickness. During the optimization cycle, a total of 71 process simulations have been run in order to evaluate gradients of the objective function with respect to each preform design variable. These gradients are fed to a commercial software library (Vanderplaats Research & development) in order to evaluate the search direction, via a SQP method.

Figures 12 and 13 show that the initial preform design was under-designed. This is due to the fact that the con-
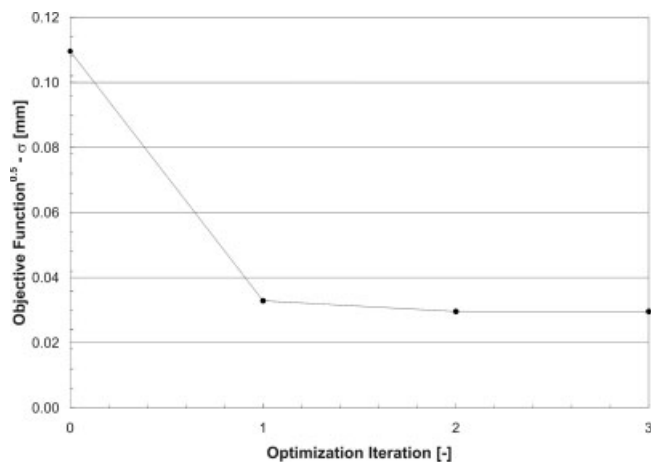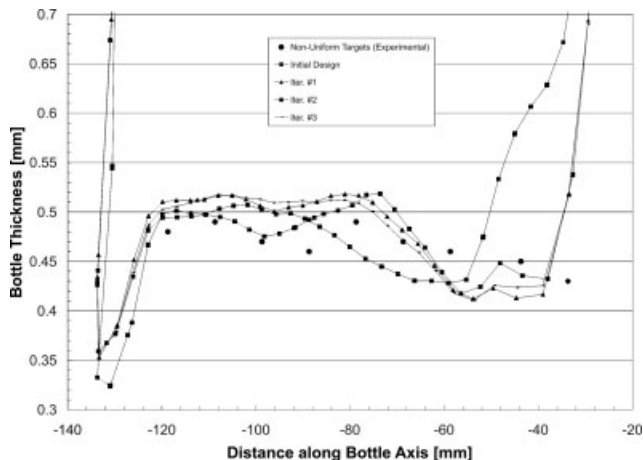
tainer thickness profile is much lower than the container thickness targets. As the optimization progresses, the container thickness profile increases and gets closer to the thickness targets. The optimal preform geometry obtained satisfies all the process constraints (Eq. 17).

Figure 14 compares the preform thickness and shape for the predicted optimal and experimental Husky designs. In the same figure, both preform geometries are superimposed. As shown, the optimal preform geometry is very close to the Husky design. However, the optimal preform thickness is less in overall magnitude than the Husky design, predominantly in the body section. The difference is related to the fact that the radii in the preform taper section and more significantly the preform end-cap parameterization were not taken into account.

In this work, the end-cap has been parameterized using a hemi-spherical shape instead of a flat end-cap shape as used by Husky. The higher optimal preform length will lead to a smaller axial blow ratio. Since the same level of total blow-up ratio has to be reached for both designs, then the preform

FIG. 16. Objective function evolution in function of optimization iteration for the first process optimization.
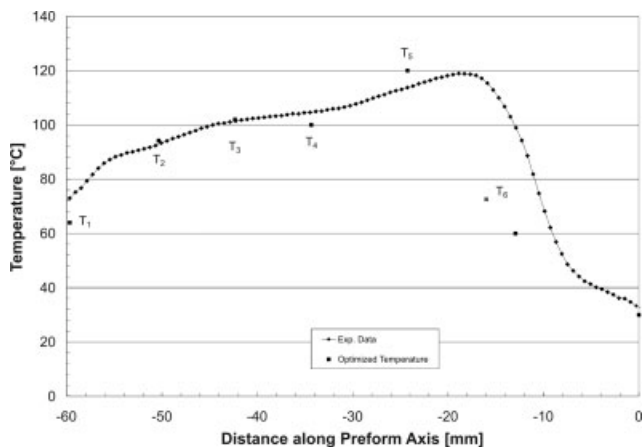

FIG. 18. Comparison between experimental and optimal preform temperature along the preform.

TABLE 5. Definition of initial temperature design variables and design variable limits (lower and upper bounds) for the process optimization.

Design variable name	Lower bound	Initial value	Upper bound
Preform temperature at position 1, X_1 (°C)	40.0	65.0	120.0
Preform temperature at position 2, X_2 (°C)	70.0	95.0	120.0
Preform temperature at position 3, X_3 (°C)	80.0	95.0	120.0
Preform temperature at position 4, X_4 (°C)	80.0	105.0	120.0
Preform temperature at position 5, X_5 (°C)	80.0	105.0	120.0
Preform temperature at position 6, X_6 (°C)	60.0	75.0	120.0
Stretching rod speed, X_7 (m/s)	0.25	0.43	0.55
Pre-blow pressure, X_8 (MPa)	0.2	0.345	0.50

thickness in the body section has to be lower for the optimal design to get an equivalent thickness distribution along the container. This explains why the optimized preform weight (18.3 g) is lower than the one manufacture by Husky (22 g).

Operating Condition Optimization

For the first optimization, the objective is to predict the optimal preform temperature distribution (Fig. 15) prior to entering the blowing station, while keeping all other processing parameters constant. This will allow for comparing the optimal preform temperature against the experimental infrared preform temperature. The initial design variables and the design variable limits are listed in Table 3. The lower bounds have been chosen to depict strain-hardening effects and the upper bounds to depict minimal blowouts. The results are illustrated in Table 4 and Figs. 16–18. The objective function decreases very rapidly after the first optimization iteration and flattens out for the next two consecutive iterations. As can be seen in Fig. 17, the initial container thickness profile is close to thickness targets, with the exception of two targets near the bottle shoulder. To improve the design in that area, the optimization algorithm has modified significantly the fifth preform temperature (X_5) located in the middle of the taper section. This preform temperature moves from 105°C up to the upper bound 120°C, allowing a higher preform stretching to target a lower container thickness.

In Fig. 18, the optimal preform temperature has the same trend and is close to the experimental preform temperature

TABLE 6. Comparison between initial and optimal processing parameters.

| Design variable name	Initial design	Optimal design
Preform temperature at position 1, X_1 (°C)	65.0	60.4
Preform temperature at position 2, X_2 (°C)	95.0	90.3
Preform temperature at position 3, X_3 (°C)	95.0	100.0
Preform temperature at position 4, X_4 (°C)	105.0	100.0
Preform temperature at position 5, X_5 (°C)	105.0	120.0
Preform temperature at position 6, X_6) (°C)	75.0	70.2
Stretching rod speed, X_7 (m/s)	0.43	0.69
Pre-blow pressure, X_8 (MPa)	0.345	0.25
Square root of objective function, σ (mm)	0.104	0.028
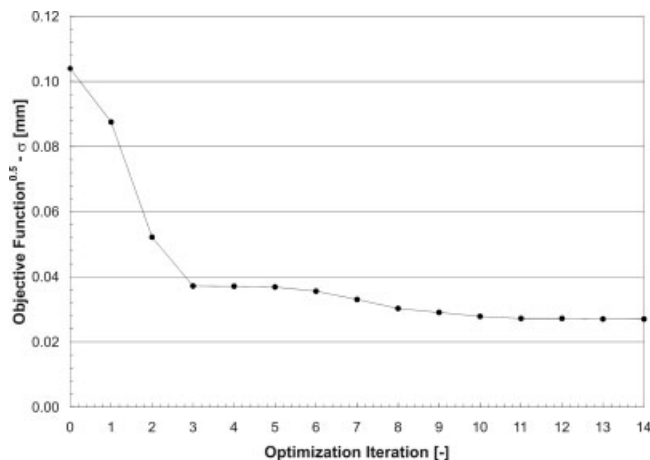
FIG. 19. Objective function evolution in function of optimization iteration for the second process optimization.

measurements with the exception of the first (T_1) and the last preform temperature (T_6). These two measurement points probably have a high level of uncertainty, since they are located at the extremity of the infrared picture, as seen in Fig. 8. Edge effects due to cooling are predominant at extremities.

The next optimization investigated was the simultaneous manipulation of several processing parameters such as the preform temperature profile, the pressure profile, and the stretching rod speed. This allows for evaluation of which design variable has the higher sensitivity effect of the final design. A preliminary study has revealed that the perturbation of the final blow pressure was not very sensitive in affecting the container thickness profile, since the container inflation is almost completed after the preblow stage. The initial design variables and the design variable limits are shown in Table 5. The results are illustrated in Table 6 and Figs. 19–22. Since more design variables are involved in this constrained optimization, the convergence is obtained after 14 optimization iterations (Fig. 19), which requires
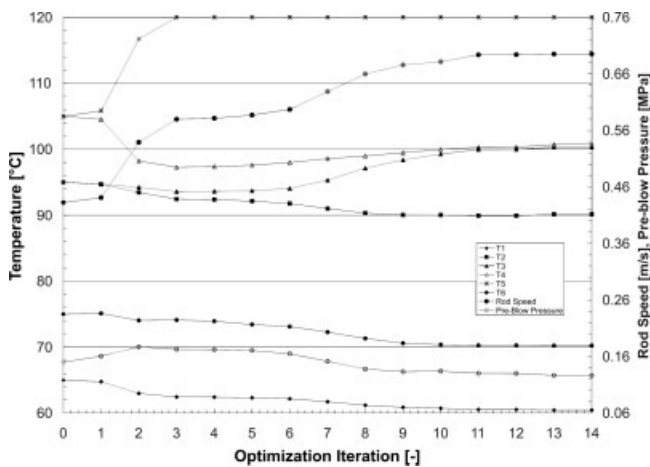

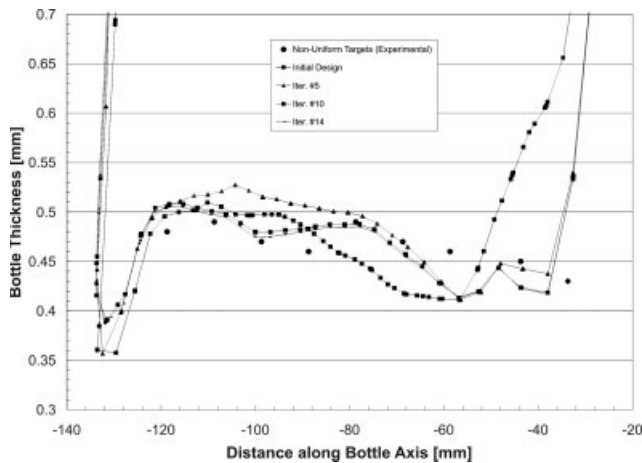FIG. 20. Design variables history for the second process optimization.

FIG. 21. Evolution of container thickness distribution in function of optimization iteration for the second process optimization.

288 process simulations (total CPU time of 1872 min or 31.2 h, i.e. 6.5 min CPU time per simulation on a 2.5 GHz PC computer running on Linux environment).

Comparison to the previous optimization where only preform temperature was manipulating shows that the better design has been obtained since the standard deviation (σ, square root of the objective function) went down to 0.028 mm compared to 0.032 mm for the previous one. In Fig. 21, good agreement has been obtained between the optimal container thickness profile at Iteration 14 and the experimental thickness targets. The optimization improves the thickness profile close to the container shoulder. In Fig. 20, design variables that have been modified significantly are the preform temperature point T_5 and the stretching rod speed. Concerning the comparison between the optimal and experimental preform temperature profile, no significant improvement has been observed. Consequently, the stretching rod speed can be identified as a parameter to manipulate to get a better design.
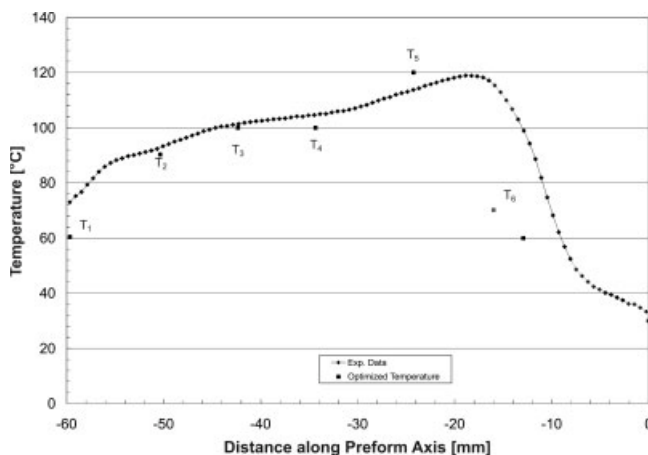

FIG. 22. Comparison between experimental and optimal preform temperature along the preform.

CONCLUSION

In this work, a new design environment has been developed to automatically design a new preform geometry for given processing conditions or optimize the operating conditions for a given preform geometry of a SBM process. The preform geometry has been parameterized based on design mathematical rules used by Amcor Company. A new optimization methodology, based on DOT technology, has been developed to manipulate the preform geometry (shape and thickness) and the operating conditions to target a require container thickness distribution along the container. Both algorithms have been tested on industrial case of Husky IMS to

- Optimize the preform geometry (shape and thickness) for given processing parameters to target the experimental container thickness profile along the container.
- Optimize the processing parameters for given preform geometry to target the experimental container thickness profile along the container.

All optimizations performed have converged and allowed to improve the design significantly. The optimization algorithm developed is a powerful tool to minimize the preform design development time and minimize the tooling reworks.

REFERENCES

1. Moldflow Documentation, http://www.moldflow.com/stp/english/products/mpa/mpa_opt_tools.htm.
2. D.K. Lee and S.K. Soh, *Polym. Eng. Sci.*, **36**(11), 1513 (1996).
3. D. Laroche, R.W. DiRaddo, and L. Pecora, in *Proceedings of the Fifth International Conference on Numerical Methods in Industrial Forming Processes—NUMIFORM*, June, 1041 (1995).
4. C. Gauvin, F. Thibault, and D. Laroche, *Polym. Eng. Sci.*, **43**(7), 1407 (2003).
5. D.E. Smith, C.J. Chen, M. Usman, and J. Koskey, *ASME*, **227**, 259 (1997).
6. K.K. Kabanemi, J.-F. Hétu, and A. Derdouri, *Design Sensitivity Analysis Applied to Injection Molding for Optimization of Gate Location and Injection Pressure*, NRC, Boucherville, 2002.
7. H. Naceur, *Contribution à l'optimisation de forme de structures minces en presence de non linéarités géométriques et matérielles*, Ph.D. Thesis, Université de Technologie de Compiègne (1998).

8. A. Srikanth and N. Zabarasm, *Comput. Methods Appl. Mech. Eng.*, **190**(13), 1859 (2000).

9. Z.Y. Goa and R.V. Grandhi, *Int. J. Numerical Methods Eng.*, **45**(10), 1349 (1999).

10. H. Ou, C.G. Armstrong, and M.A. Price, *J. Mater. Process. Technol.*, **132**, 21 (2003).

11. X. Zhao, G. Zhao, G. Wang, and T. Wang, *J. Mater. Proc. Tech.*, **128**, 25 (2002).

12. H. Shim, *J. Mater. Proc. Tech.*, **134**, 99 (2003).

13. G.A. Giles and D.R. Bain, *Technology of Plastics Packaging for the Consumer Market*, Sheffield Academic Press, 259 (2001).

14. G.N. VanderPlaats, *Numerical Optimization Techniques for Engineering Design*, VanderPlaats Research & Development, Colorado Springs, Colorado (1999).

15. T. Pham, F. Thibault, and L.-T. Lim, *Polym. Eng. Sci.*, **44**(8), 1460 (2004).

16. R. DiRaddo, D. Laroche, and B. Brace, *SPE ANTEC Technical Paper*, Dallas, USA (2001).

17. M. Yousefi, R. DiRaddo, and A. Bendada, *Polymer Processing Society 17*, Montreal, Canada (2001).

18. D. Laroche, K. Kabanemi, L. Pecora, and R. DiRaddo, *Polym. Eng. Sci.*, **39**(7), 1223 (1999).